PHYSICAL REVIEW B **84**, 140408(R) (2011)

Directional short range order in $L1_0$ FeMnPt magnetic thin films

Cheng-Jun Sun,[1,*] Dongbin Xu,[1,2] Steve M. Heald,[1] Jingsheng Chen,[2] and Gan-Moog Chow[2,†]
[1]*Advanced Photon Source, Argonne National Laboratory, Argonne, Illinois 60439, USA*
[2]*Department of Materials Science and Engineering, National University of Singapore, Singapore 117576*
(Received 16 September 2011; published 18 October 2011)

A method for investigating the directional short range order (DSRO) of an element of interest in $L1_0$ FeMnPt thin films using polarization-dependent x-ray absorption near edge structure (XANES) spectroscopy is described. The XANES calculations for both $L1_0$ FePt and $L1_0$ MnPt phases indicate that the height of the low-energy shoulder of the polarization-dependent XANES is proportional to the degree of DSRO of the element of interest in the case of $L1_0$ FePt and MnPt systems. The experimentally observed DSROs of Fe and Mn in $L1_0$ FeMnPt magnetic thin films are consistent with a decrease of ordering parameter with increasing Mn doping. We demonstrate theoretically and experimentally that the heights of the low-energy shoulder in the Fe*K*- and Mn*K*-edge polarization-dependent XANES are proportional to the DSROs of Fe and Mn, respectively.

DOI: 10.1103/PhysRevB.84.140408 PACS number(s): 75.70.Ak, 61.05.cj, 75.40.−s, 78.40.Kc

The properties of magnetic thin films depend on both long range order (LRO) and short range order (SRO), especially the directional short range order (DSRO),[1] which is the SRO in a specific lattice direction. The strong spin-lattice interaction in magnetic materials often leads to either alignment or antialignment of the neighboring spins, thus giving rise to ferromagnetic (FM) or antiferromagnetic (AFM) phases.[2] The role of DSRO, such as the elemental specific coordination number at a given lattice direction, is essential to understand the complexity of antiferromagnetism and ferromagnetism in a system with a coexistence of AFM and FM phases. In particular, one would expect that a change in the magnetic properties could be large when the DSRO is changed.[3]

A model system for this Rapid Communication is the $L1_0$ FeMnPt phase, which is well known for the coexistence of the $L1_0$ FM FePt and $L1_0$ AFM MnPt phases.[4] The magnetic and electronic properties with models of various spin configurations in $L1_0$ ordered MnPt and FePt alloys were investigated theoretically using first-principles theory.[5] The relative energies with respect to those of the most stable magnetic moment direction for a give model are compared, as shown in Fig. 1. It has been theoretically demonstrated that the most stable phase of $L1_0$ MnPt is AFM, with all the spins within the (001) plane[5] aligning in an alternating chessboard arrangement and with a FM spin arrangement between adjacent (001) planes. In contrast, $L1_0$ FePt is a FM phase with a stable status of all spins aligning perpendicular to the (001) direction. In this Rapid Communication, the DSRO of Fe and Mn is defined as the fraction of Fe-Fe bonds and Mn-Mn bonds in a given lattice plane or direction. Therefore, the fraction of an AFM phase or (and) FM phase in $L1_0$ FeMnPt is associated to the DSRO of Fe and Mn, both parallel and perpendicular to the (001) plane. However, to the best of our knowledge, little is known about the DSRO in $L1_0$ FeMnPt (001) magnetic thin films from either theoretical or experimental points of view.

DSRO has been previously investigated using a polarization-dependent extended x-ray absorption fine structure (EXAFS).[6,7] However, EXAFS is not an appropriate tool for investigating materials consisting of elements with similar lattice parameters, backscattering amplitudes, and phase shifts,[8] such as Mn and Fe. In this Rapid Communication, we demonstrate theoretically and experimentally that in $L1_0$ FeMnPt magnetic thin films the low-energy features in the Fe*K*- and Mn*K*-edge polarization-dependent XANES spectra increase with increasing DSROs of Fe and Mn, respectively. Building on the combination of XANES experiments and simulations, we establish that the degree of DSRO of the specific element is proportional to the height of a low-energy feature just above the absorption edge in the case of Fe or Mn in $L1_0$ FeMnPt magnetic thin films. Subtle changes already show up in FeMnPt films for Mn doping from 10 to 15 at.% in both Mn and Fe XANES spectra with the x-ray polarization parallel ($E \parallel$ surface) and perpendicular ($E \perp$surface) to the $L1_0$ FePt (001) surface plane. Based on the DSRO results, a model of structural evolution as a function of Mn doping is proposed, which is also consistent with the observed LRO and magnetic properties. The qualitative investigation of DSRO by a combination of the XANES analysis and the first-principle calculation developed here may provide a general method of study of DSRO in thin films measured with x-ray polarization parallel and perpendicular to the surface plane. This method may also be extended to investigate the DSRO at any given lattice direction in other materials systems.

$Fe_{(50-x)}Mn_xPt_{50}$ films (50 nm) with Mn concentrations of $x = 0$, 10, and 15 at.% were deposited using sputtering onto single-crystal MgO (100) substrates at 550 °C. The details of the sample fabrication and basic magnetic and structural properties were reported elsewhere.[9] In summary, all the films were epitaxially grown through the relation of MgO (001) ⟨100⟩ $\parallel$ $L1_0$ FePt (001) ⟨100⟩, and exhibit perpendicular magnetic anisotropy. The $L1_0$ ordering parameter, perpendicular magnetic anisotropy, and saturation magnetization (M_s) of the films decrease with the increase in the atomic percentage of Mn doping. In particular, the sharp decrease of M_s with Mn doping was suggested to be associated with the formation of an AFM $L1_0$ MnPt phase.

The XANES measurements were performed using linear polarized x rays at the undulator beamline 20-ID-B of the Advanced Photon Source (APS), Argonne National Laboratory. Details on the beamline optics and instruments can be found elsewhere.[10] In particular, the microprobe station

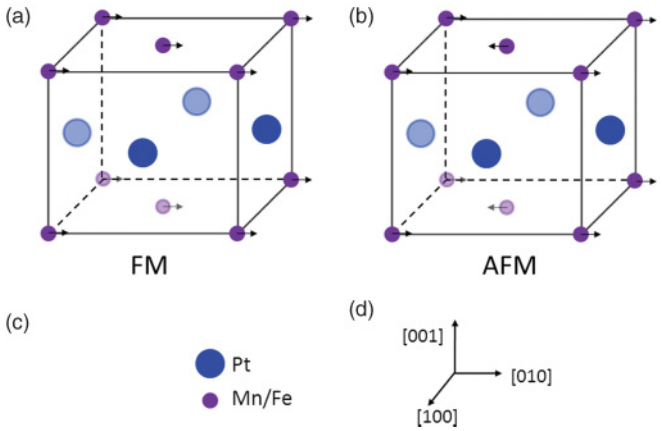

FIG. 1. (Color online) Models of $L1_0$ ordered FePt or MnPt alloy. (a) A ferromagnetic (FM) type $L1_0$ ordered alloy. (b) An antiferromagnetic (AFM) type $L1_0$ ordered alloy. (c) The large blue filled circles are Pt atoms, and the small purple filled circles are Fe or Mn atoms. (d) The lattice directions of the $L1_0$ structure. The details of the models are discussed in Ref. 5.

was used to provide a focused beam size of 3 μm, allowing glancing angle measurements with x-ray polarization parallel and perpendicular to the (001) surface plane. Fe and Mn metal foils placed to intercept a scattered beam were used as an online check of the monochromator energy calibration.[11] The absorption edge positions for Fe and Mn were taken as 7110.75 and 6537.67 eV, respectively.[12]

Due to the linear polarized x ray, the x-ray absorption coefficient will show a polarization dependence for an anisotropic sample such as the $L1_0$ ordered FeMnPt films as illustrated in Eq. (1):[7]

$$u(\theta) = u_{\parallel} + (u_{\perp} - u_{\parallel})\cos^2\theta, \tag{1}$$

where θ is the angle between the polarization vector and surface normal, and $u_{\parallel}$ and $u_{\perp}$ are the absorption coefficients with polarization vector parallel or perpendicular to the surface of the sample. Furthermore, the K and L_1 shell polarization factor $p(e)$ that accounts for the polarization of the incoming x rays can be written as[7]

$$p(e) = 3\cos^2\theta. \tag{2}$$

If the materials have random orientations or have cubic or higher symmetry, then $\cos^2\theta = 1/3$ and $p(e)$=1. The absorption coefficient of powder-average spectra $u_{\text{isotropic}}$, which in this case assume the FeMnPt films are randomly oriented, can be written by substituting $\cos^2\theta = 1/3$ in Eq. (1) as follows:

$$u_{\text{isotropic}} = \tfrac{2}{3}u_{\parallel} + \tfrac{1}{3}u_{\perp}. \tag{3}$$

In this Rapid Communication, the powder-average spectra, which are 1/3 of the perpendicular orientation signal plus 2/3 of the parallel orientation signal,[7,13] of the films at the Fe and Mn K edges are shown in Figs. 2(a) and 2(c), respectively. The XANES of Fe metal foil has a low-energy shoulder A near 7114 eV, a medium-energy shoulder B near 7121 eV, and a high-energy peak C at 7129 eV; the XANES of Mn metal foil gives rise to a low-energy shoulder A near 6540 eV and a high-energy peak C at 6555 eV. The low-energy shoulder A can be assigned to a p-projected density of states hybridized with the 3d states of the surrounding atoms.[14,15] Figures 2(b) and 2(d) show the first derivative of the Fe and Mn absorption edges. Peak E is used to define the absorption edge energy, and peak F defines the position of the low-energy shoulder A. The heights of low-energy shoulder A at both the Fe K edge [Fig. 2(a)] and the MnK edge [Fig. 2(c)] increase when the respective element composition increases in the thin films. Assuming the Fe and Mn is uniformly distributed in the epitaxial-grown thin films, the increase in Fe or Mn composition is associated with an increasing fraction of Fe-Fe and Mn-Mn bonds; thus, the height of the low-energy shoulder at the Fe K or MnK edges can be related to the degree of SRO in the Fe-Fe or Mn-Mn bonding.

Why does the height of the low-energy shoulder at the FeK or MnK edge increase when the SRO of Fe-Fe or Mn-Mn is increased? The increase of the height of a similar low-energy shoulder with an increase of its corresponding elemental composition has been found in various cases. For example, the heights of the low-energy shoulders of Fe and Ni decrease when the compositions of Fe and Ni are reduced in FeNi alloys,[14] the height of a low-energy shoulder of Cu increases as the Cu composition is increased in the CuPt (Ref. 16) and CuAu (Ref. 17) alloys, and the height of the low-energy shoulder of Fe declines when the thickness of Fe in a $[Fe/Si_3N_4]_n$ multilayer is decreased.[18] Although a complete interpretation of the correlation between the height of the low-energy shoulder and the constituting elemental composition is still lacking, these examples reflect the mounting evidence that the height of a low-energy shoulder might be proportional to the SRO for the 3d transition metals. As pointed out above, the low-energy shoulder is associated with a p-projected density of states hybridized with the 3d states of the surrounding atoms,[14,15] so the increase of the SRO of Fe-Fe or Mn-Mn would result in a decrease of the hybridization, giving rise to an increase of unoccupied states. Therefore, the height of the low-energy shoulder becomes more pronounced.

Is the height of the low-energy shoulder of the polarization-dependent XANES proportional to the DSRO of the element of interest? To answer this, both polarization-dependent XANES experiments and simulations were employed to study the correlation of DSRO and the height of the low-energy shoulder at its absorption edge.

The XANES spectra with the x-ray polarization parallel and perpendicular to the $L1_0$ FePt (001) lattice plane were calculated using the *ab initio* FEFF8.4 code.[19] Specifically, a cluster of 103 atoms with a size of 7 Å was applied for the calculation of full-multiple scattering (FMS), a cluster of 55 atoms with a size of 5.5 Å was used for the calculation of the self-consistent-field (SCF) muffin-tin atomic potential, and a Hedin-Lundqvist exchange potential of 2.0 eV was chosen to account for the broadening of the spectra.

Figure 3 displays the calculated FeK-edge [Fig. 3(a)] and MnK-edge [Fig. 3(b)] XANES, both parallel and perpendicular to the $L1_0$ FePt (001) plane. The isotropic spectrum for unpolarized x rays is also shown as a reference. The lattice parameters of $L1_0$ $Fe_{50}Pt_{50}$ films here were applied in the calculation for both FeK and MnK edges. The calculated XANES spectra at both the FeK edge [Fig. 3(a)] and MnK edge

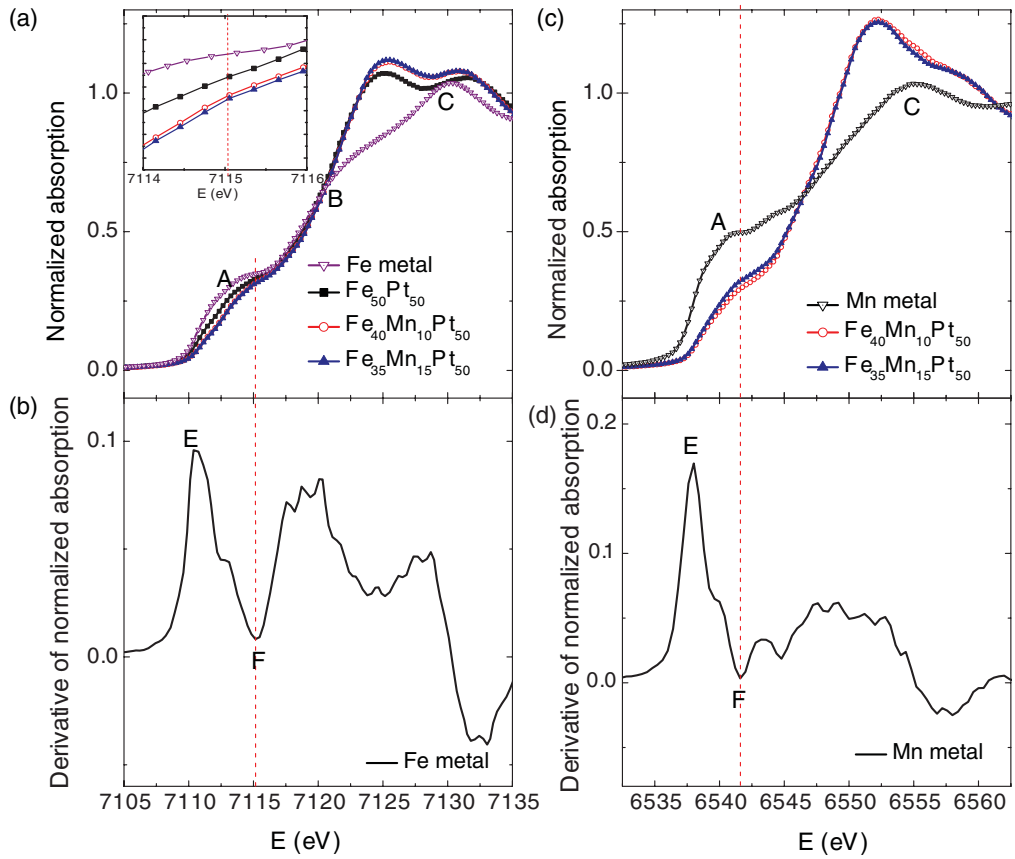

FIG. 2. (Color online) Measured XANES spectra consisting of 1/3 of the perpendicular orientation signal plus 2/3 of the parallel orientation signal. (a) XANES spectra at the Fe*K* edge for Fe metal and FeMnPt films: The difference between the $Fe_{40}Mn_{10}Pt_{50}$ and $Fe_{35}Mn_{15}Pt_{50}$ can be found in the inset of (a). (b) The derivative of the XANES spectrum of Fe metal foil. (c) XANES spectra at the Mn*K* edge for Mn metal and FeMnPt films. (d) The derivative of the XANES spectrum of Mn metal foil. A, B, and C in (a) and (c) denote the low-energy shoulder, medium-energy shoulder, and high-energy peak, respectively. E and F in (b) and (d) correspond to the absorption edge and the first negative peak, respectively.

[Fig. 3(b)] indicate a significant polarization dependence; the height of the low-energy shoulder of the parallel spectrum is higher than that of the perpendicular one, with the isotropic spectrum in between. For an ideal $L1_0$ ordered phase there is complete directional short range order, and the signal of the parallel XANES mainly results from the Fe-Fe bonds in the (001) plane, whereas the perpendicular XANES is caused by a combination of Fe-Pt and Fe-Fe bonds in the [001] direction.

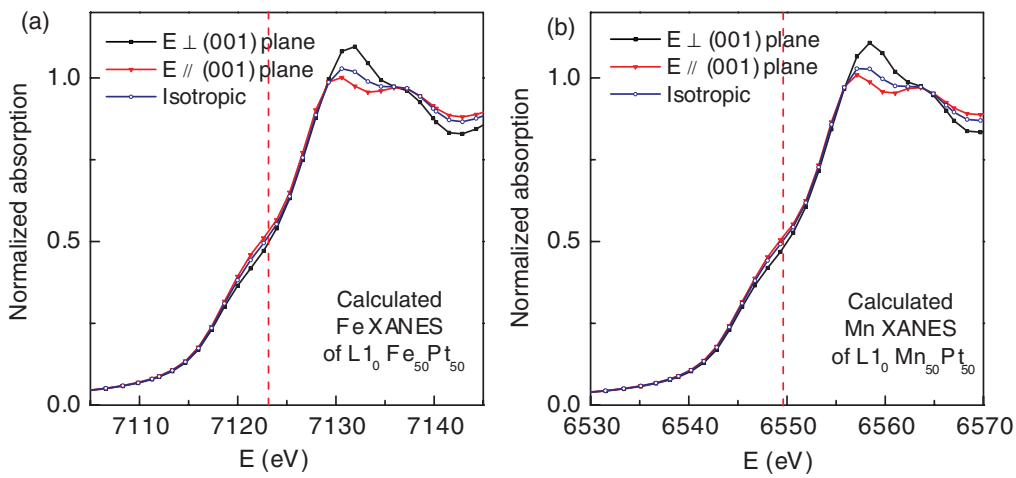

FIG. 3. (Color online) Calculated XANES spectra. (a) The calculated polarization-dependent XANES spectra of $L1_0$ $Fe_{50}Pt_{50}$ using the *ab initio* FEFF8.4 code at the Fe*K* edge. (b) The calculated polarization-dependent XANES spectra of $L1_0$ $Mn_{50}Pt_{50}$ using *ab initio* FEFF8.4 at the Mn*K* edge. The isotropic XANES spectra without polarization dependence are displayed as a reference.

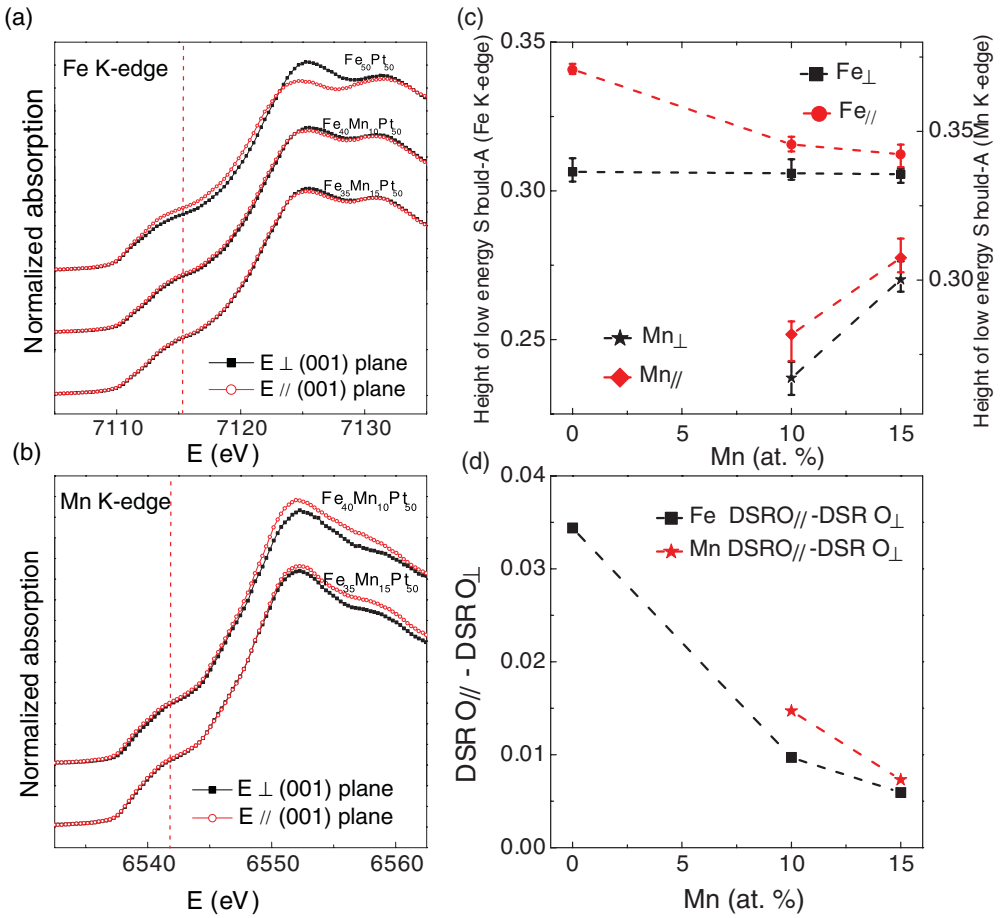

FIG. 4. (Color online) Measured polarization-dependent XANES spectra. (a) Polarization-dependent XANES spectra of FeMnPt films at the Fe*K* edge. Five separate measurements are used to obtain the averaged Fe XANES. (b) Measured polarization-dependent XANES spectra of FeMnPt films at the Mn*K* edge. Four separate measurements are used to obtain the averaged Mn XANES. (c) The intensity of low-energy shoulders as a function of Mn composition. The error bars were obtained by comparing the averaged XANES with the individual scans. (d) The difference DSRO ($DSRO_{\parallel} - DSRO_{\perp}$) of Fe and Mn as a function of the Mn composition.

The isotropic spectrum consists of 1/3 of the perpendicular orientation signal plus 2/3 of the parallel orientation signal. The sequence of the degree of DSRO of Fe from high to low is parallel to the (001) plane, the isotropic, and perpendicular to the (001) plane, which is the sequence of the height of the low-energy shoulders for the simulated spectra [Fig. 3(a)]. A similar result is found from the XANES calculation of the polarization-dependent $L1_0$ MnPt ordered phase. The XANES calculations for both $L1_0$ FePt [Fig. 3(a)] and $L1_0$ MnPt [Fig. 3(b)] phases indicate that the height of the low-energy shoulder of the polarization-dependent XANES is proportional to the degree of DSRO of the element of interest in case of $L1_0$ FePt and MnPt systems. Furthermore, our calculations of polarization-dependent XANES spectra for the $L1_0$ ordered phase are also consistent with other XANES calculations for the $L1_0$ ordered FePt (Ref. 20) and CoPt (Ref. 21) phases. By comparing earlier work with our calculation, similarities can be found in both the shape and the height of the low-energy shoulder, but the DSRO was not specifically discussed in these studies.[20,21]

Figure 4 displays the polarization-dependent XANES measurements for the FeMnPt films at both the Fe [Fig. 4(a)] and Mn*K* edges [Fig. 4(b)], respectively. The heights of the low-energy shoulder A and difference in the low-energy shoulder A between parallel and perpendicular XANES measurements are shown in Figs. 4(c) and 4(d). While the error bars in the heights of the features for the Mn*K* edge and their differences are relatively large, the results suggest that the trend of differences of DSRO in Mn as a function of Mn composition follows that of Fe, indicating that the Mn is substituting into Fe sites in the FePt films. Subtle changes already show up in FeMnPt films when the Mn doping increases from 10 to 15 at.% for both the Mn and Fe XANES spectra. Comparing the DSRO of Mn in the $Fe_{40}Mn_{10}Pt_{50}$ and $Fe_{35}Mn_{15}Pt_{50}$ films, the difference of DSRO for Mn at $Fe_{40}Mn_{10}Pt_{50}$ films is larger than that of $Fe_{35}Mn_{15}Pt_{50}$, though the Mn doping is lower in the $Fe_{40}Mn_{10}Pt_{50}$ films compared to that of $Fe_{35}Mn_{15}Pt_{50}$ films. These observed DSROs (Fig. 4) are consistent with a decrease of ordering parameter with increasing Mn doping.[9] In addition, the finding that $DSRO_{\perp}$ of Fe is constant as a function of the Mn content can be understood as follows: When the Mn content increases, the $L1_0$ ordering decreases; on the one hand, a decrease in $L1_0$ ordering increases the $DSRO_{\perp}$ of Fe, and on the other hand, an increase in Mn content decreases the $DSRO_{\perp}$ of Fe as a result of a decrease in the total Fe content in the films—consequently, the $DSRO_{\perp}$

of Fe can be constant as a function of the Mn content due to the combined effects. In a separate study on the polarization dependence of the XANES spectra of an Fe layer on the GaAs surface,[22] the low-energy shoulder reduces in both the parallel and perpendicular directions when the number of Fe monolayers is decreased. As reducing the number of Fe monolayers results in a decrease in the DSRO of Fe in both directions, the observation of a decrease in the low-energy shoulder with a decrease in the thickness of the Fe monolayer can be understood as due to a decrease in the DSRO of Fe in both directions, offering solid experimental support for this study. The combination of theoretical calculations of XANES spectra (Fig. 3) and polarization-dependent XANES measurements (Fig. 4) suggests that the low-energy shoulder could be used to study the DSRO of the element of interest in the case of Fe or Mn in $L1_0$ FeMnPt magnetic thin films.

The observed magnetic properties of the FeMnPt films and the $L1_0$ ordering, obtained from LRO characterization as a function of Mn composition in this work[9] also verify the DSRO of Fe and Mn obtained by the polarization-dependent XANES experiments and calculations. As discussed above, the most stable phase for $L1_0$ MnPt is an AFM phase with AFM ordering in the (001) plane, and FM ordering between the (001) planes (Fig. 1). $L1_0$ FePt is a FM phase with a stable status of all spins aligning perpendicular to the (001) direction (Fig. 1). Based on the DSRO analysis, the structural evolution as a function of Mn doping is suggested as follows: Mn is substituting into the Fe site in $L1_0$ FeMnPt films, and the DSRO of Mn follows the DSRO of Fe; the difference in DSRO of both Fe and Mn decreases as the Mn doping increases, however, the absolute amount of parallel DSRO of Mn within the (001) lattice plane in $Fe_{35}Mn_{15}Pt_{50}$ is much higher than that of Mn in $Fe_{40}Mn_{10}Pt_{50}$ [Fig. 4(c)]. As shown in Fig. 1, the magnetic spin of the Mn atom prefers to align antiferromagnetically with the magnetic spin of neighboring Mn atoms within the (001) lattice plane to minimize the total energy, thus forming an AFM phase.[5] Accordingly, the accumulation of AFM phase in the (001) plane when the Mn doping is increased leads to a sharp decrease of M_s.[9]

In summary, a method is described which investigates the DSRO of an element of interest using polarization-dependent XANES spectroscopy. We demonstrate theoretically and experimentally that the height of the low-energy shoulder in the K-edge polarization-dependent XANES in the case of Fe or Mn in $L1_0$ FeMnPt magnetic thin films is proportional to the DSRO of the element of interest.

PNC/XSD facilities at the Advanced Photon Source, and research at these facilities, are supported by the US Department of Energy–Basic Energy Sciences, a Major Resources Support grant from NSERC, the University of Washington, Simon Fraser University, and the Advanced Photon Source. Use of the Advanced Photon Source, an Office of Science User Facility operated for the US Department of Energy (DOE) Office of Science by Argonne National Laboratory, was supported by the US DOE under Contract No. DE-AC02-06CH11357. This work is partially supported by the Ministry of Education, Singapore under Grant No. R-284-000-061-112, and A*STAR under Grant No. R-284-000-082-305. The authors would like to thank Dr. R. A. Gordon for the helpful discussions.

*cjsun@aps.anl.gov

†msecgm@nus.edu.sg

[1] S. S. A. Razee, J. B. Staunton, B. Ginatempo, F. J. Pinski, and E. Bruno, Phys. Rev. Lett. **82**, 5369 (1999).

[2] J. C. Loudon, N. D. Mathur, and P. A. Midgley, Nature (London) **420**, 797 (2002).

[3] H. Bernas, J. P. Attane, K. H. Heinig, D. Halley, D. Ravelosona, A. Marty, P. Auric, C. Chappert, and Y. Samson, Phys. Rev. Lett. **91**, 077203 (2003).

[4] G. Meyer and J.-U. Thiele, Phys. Rev. B **73**, 214438 (2006).

[5] Z. H. Lu, R. V. Chepulskii, W. H. Butler, Phys. Rev. B **81**, 094437 (2010).

[6] S.-W. Han, E. A. Stern, D. Haskel, and A. R. Moodenbaugh, Phys. Rev. B **66**, 094101 (2002).

[7] S. M. Heald and E. A. Stern, Phys. Rev. B **16**, 5549 (1977); S. M. Heald, *in Characterization of Materials*, edited by E. N. Kaufmann (Wiley-Interscience, Hoboken, NJ, 2003), p. 873.

[8] G. M. Chow, W. C. Goh, Y. K. Hwu, T. S. Cho, J. H. Je, H. H. Lee, H. C. Kang, D. Y. Noh, C. K. Lin, and W. D. Chang, Appl. Phys. Lett. **75**, 2503 (1999).

[9] D. B. Xu, J. S. Chen, T. J. Zhou, and G. M. Chow, J. Appl. Phys. **109**, 07B747 (2011).

[10] S. M. Heald, J. O. Cross, D. L. Brewe, and R. A. Gordon, Nucl. Instrum. Methods Phys. Res. A **582**, 215 (2007).

[11] J. O. Cross and A. I. Frenkel, Rev. Sci. Instrum. **70**, 38 (1999).

[12] S. Kraft, J. Stumpel, P. Becker, and U. Kuetgens, Rev. Sci. Instrum. **67**, 681 (1996).

[13] S. M. Heald, T. C. Kaspar, T. Droubay, V. Shutthanandan, S. A. Chambers, A. Mokhtari, A. J. Behan, H. J. Blythe, J. R. Neal, A. M. Fox, and G. A. Gehring, Phys. Rev. B **79**, 075202 (2009).

[14] H. Sakurai, F. Ito, H. Maruyama, A. Koizumi, K. Kobayashi, H. Yamazaki, Y. Tanji, and H. Kawata, J. Phys. Soc. Jpn. **62**, 459 (1993).

[15] J. E. Müller, O. Jepsen, and J. W. Wilkins, Solid State Commun. **42**, 365 (1982).

[16] Y.-S. Lee, K.-Y. Lim, Y.-D. Chung, C.-N. Whang, and Y. Jeon, Surf. Interface Anal. **30**, 475 (2000).

[17] M. Kuhn, T. K. Sham, J.M. Chen, and K.H. Tan, Solid State Commun. **75**, 861 (1990).

[18] F. Jiménez-Villacorta, E. Céspedes, M. Vila, A. Muñoz-Martín, G. R. Castro, and C. Prieto, J. Phys. D **41**, 205009 (2008).

[19] A. L. Ankudinov, A. I. Nesvizhskii, and J. J. Rehr, Phys. Rev. B **67**, 115120 (2003).

[20] A. Martins, N. M. Souza-Neto, M. C. A. Fantini, A. D. Santos, R. J. Prado, and A. Y. Ramos, J. Appl. Phys. **100**, 013905 (2006).

[21] N. M. Souza-Neto, A. Y. Ramos, Hélio C. N. Tolentino, A. Martins, and A. D. Santos, Appl. Phys. Lett. **89**, 111910 (2006).

[22] R. A. Gordon, E. D. Crozier, D.-T. Jiang, P. S. Budnik, T. L. Monchesky, and B. Heinrich, Surf. Sci. **581**, 47 (2005).